Supplementary Materials

NMR solution structures of *Runella slithyformis* RNA 2'-phosphotransferase Tpt1 provide insights into NAD^+ binding and specificity

Sébastien Alphonse, Ankan Banerjee, Swathi Dantuluri, Stewart Shuman and Ranajeet Ghose

Supplemental Figures: S1 – S18

Supplemental Tables: S1 – S3

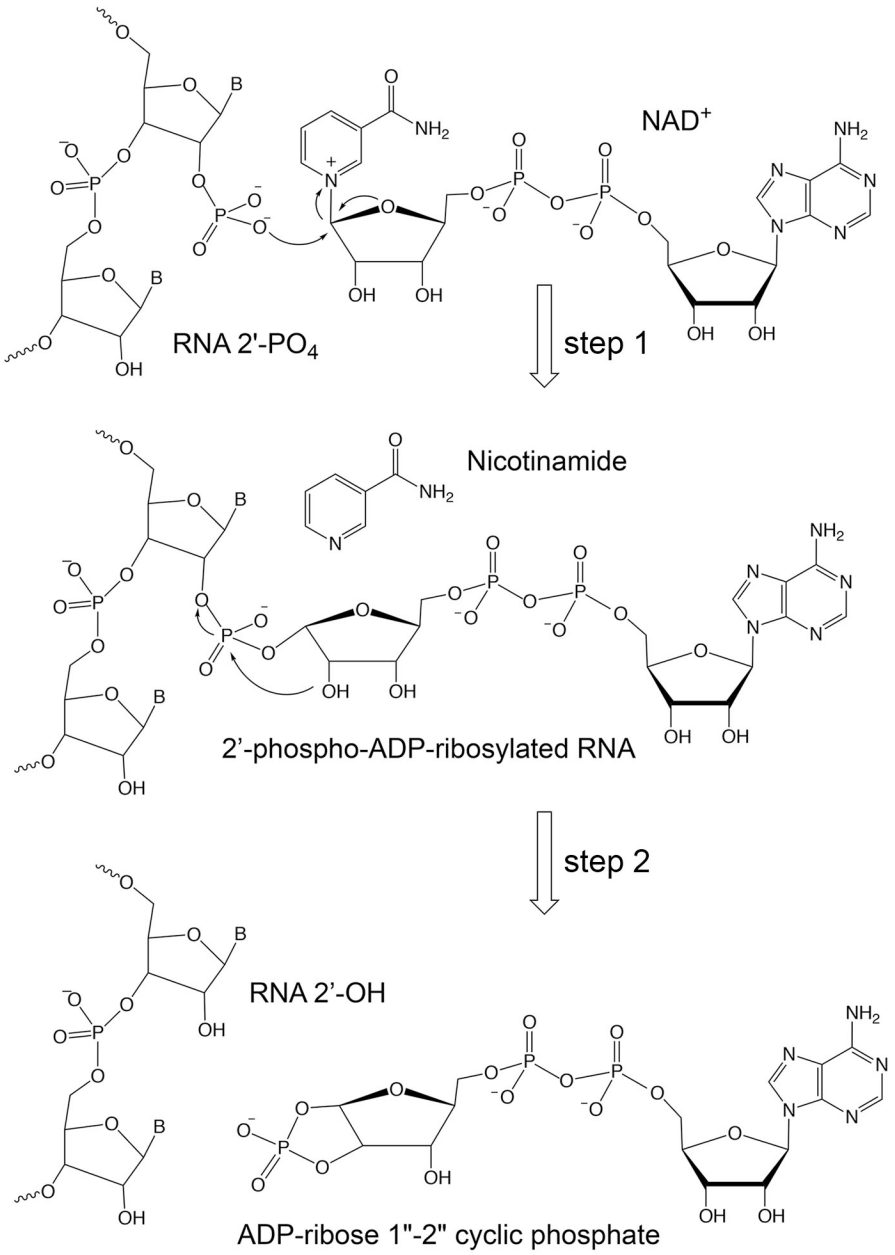

Figure S1. Two-step mechanism for the Tpt1-catalyzed removal of 2'-PO_4 from a 2'-PO_4, 3'-5' phosphodiester RNA junction. The Tpt1 reaction pathway comprises two chemical steps – Step 1: the RNA 2'-PO_4 reacts with NAD^+ to expel nicotinamide resulting in a 2'-phospho-ADP-ribosylated RNA intermediate; Step 2: transesterification of the ADP-ribose 2"-OH to the RNA 2'-PO_4 displaces the RNA 2'-OH and generates ADP-ribose-1",2"-cyclic phosphate.

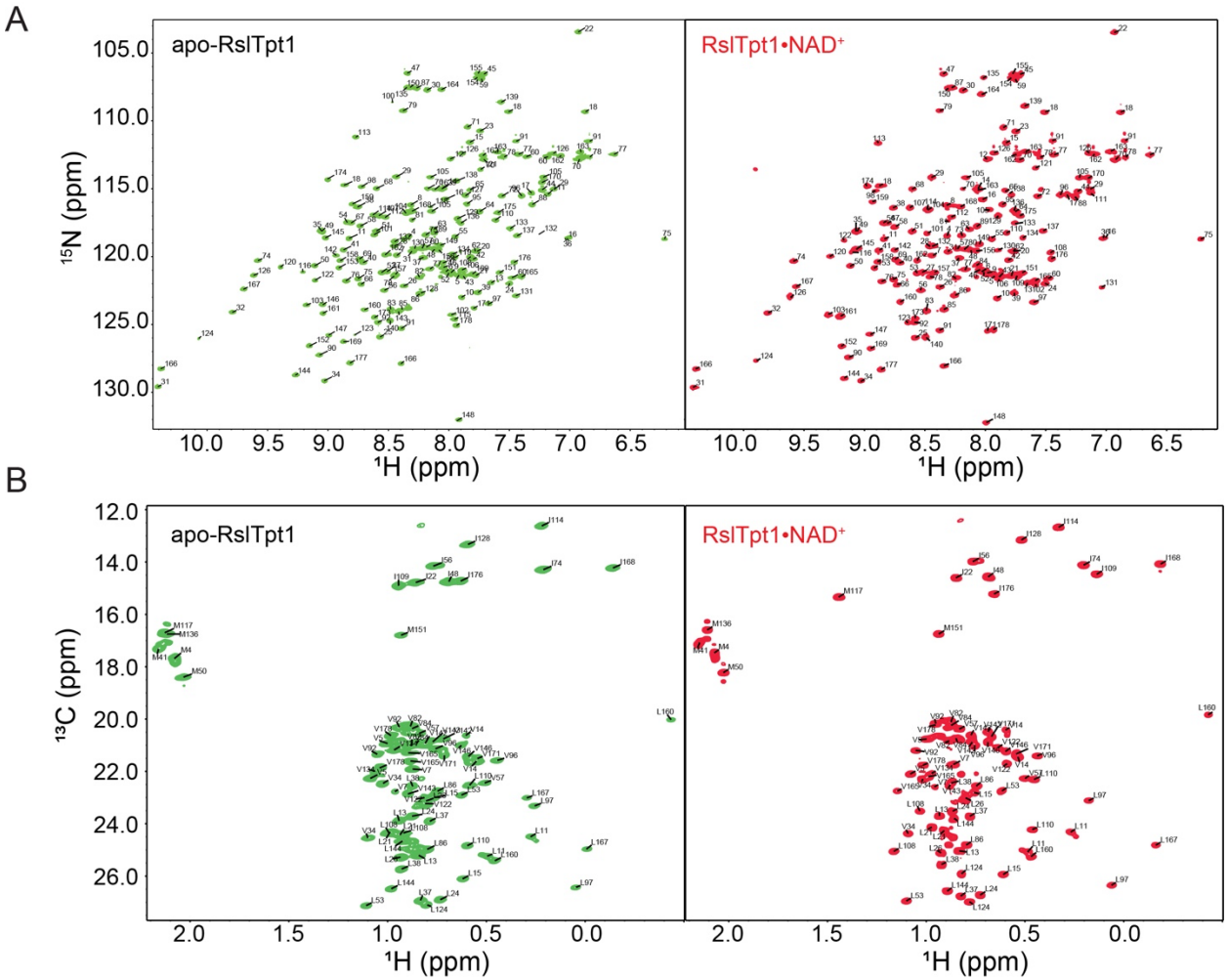

Figure S2. ^{15}N, ^{1}H HSQC spectra (900 MHz) of apo-RslTpt1 (left) and the RslTpt1•NAD^{+} complex (right) are shown in panel A. ^{13}C, ^{1}H HMQC spectra (800 MHz) of ILVM-labeled apo-RslTpt1 (left) and the RslTpt1•NAD^{+} complex (right) are shown in panel B.

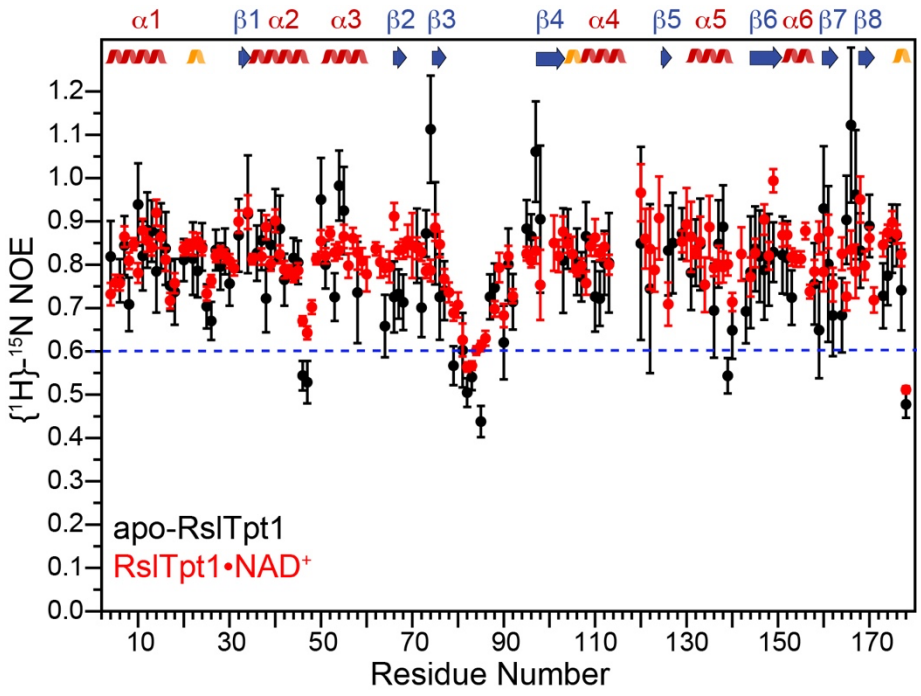

Figure S3. $\{^1H\}$-^{15}N steady state NOE values measured at 800 MHz for apo-RslTpt1 (black) and for the RslTpt1•NAD^+ complex (red) are plotted against residue number. The solid circles and the bars represent the mean and standard deviations, respectively. Given the reduced long-term sample stability of apo-RslTpt1 and the resulting lower concentration that could be used in the measurement, the NOE values have larger experimental uncertainties compared to the NAD^+-bound case. Secondary structural elements (definitions are as per apo-RslTpt1, see Table S3) are indicated; α-helices, β-strands and 3_{10}-helices are colored red, blue and gold, respectively. α-helices and β-strands are labeled.

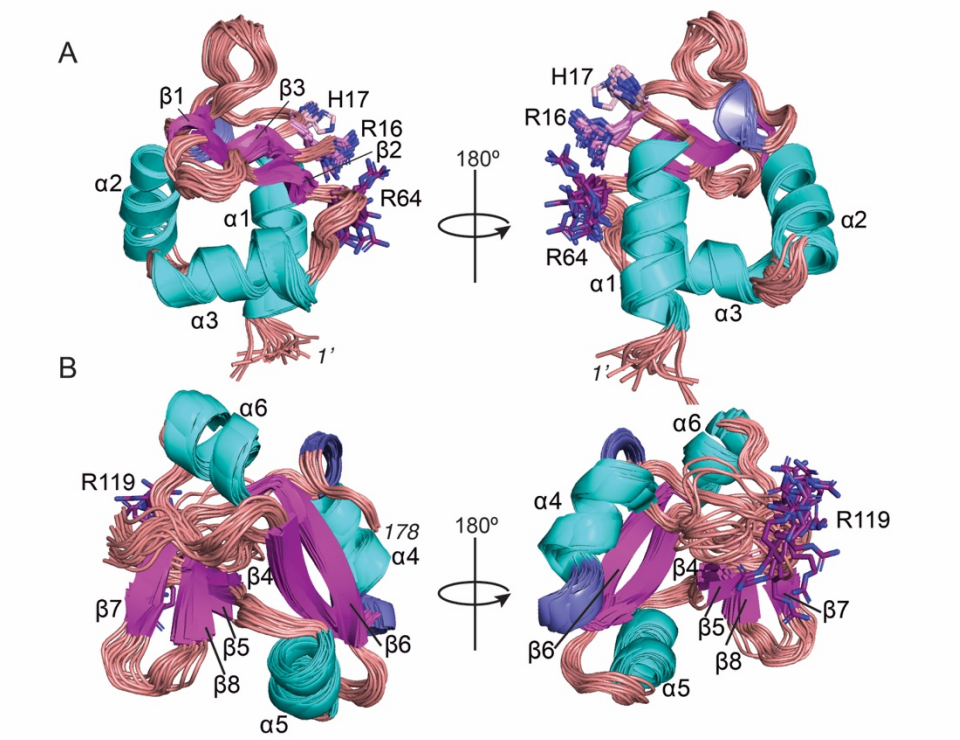

Figure S4. The 20 structures of the NMR ensemble of apo-RslTpt1 overlaid on the N-lobe (panel A) the C-lobe has been removed for ease in visualization) and the C-lobe (panel B, the N-lobe has been removed for ease in visualization). Also shown are the sidechains of the Arg-His-Arg-Arg catalytic tetrad (Arg16, His17 and Arg64 on the N-lobe, Arg119 on the C-lobe). 1' indicates the N-terminus with the first 4 amino acid residues being a remnant of the purification tag.

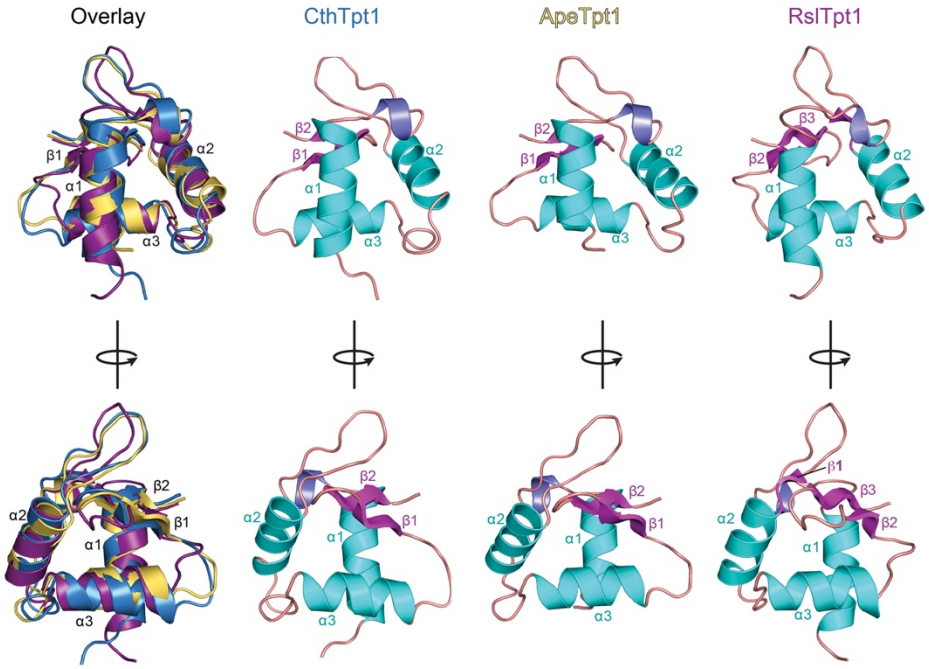

Figure S5. Comparison of the structures of the N-lobes of RslTpt1, CthTpt1 (1) and ApeTpt1 (2). The structural overlay includes residues 4-17, 19-22, 34-43, 50-59, 65-68 and 73-76 for RslTpt1; residues 6-19, 21-24, 36-45, 54-63, 69-72 and 75-78 for CthTpt1 (PDB: 6E3A, 6EDE); residues 4-15, 17-20, 32-41, 49-58, 64-67 and 70-73 for ApeTpt1 (PDB: 1WFX). The overlay includes a total of 184 backbone N, Cα, C' and O atoms. The extreme left panel shows the overlaid structures with CthTpt1 in blue, ApeTpt1 in yellow and RslTpt1 in magenta. Also shown are the individual structures in approximately the same orientation with key secondary structural elements labeled.

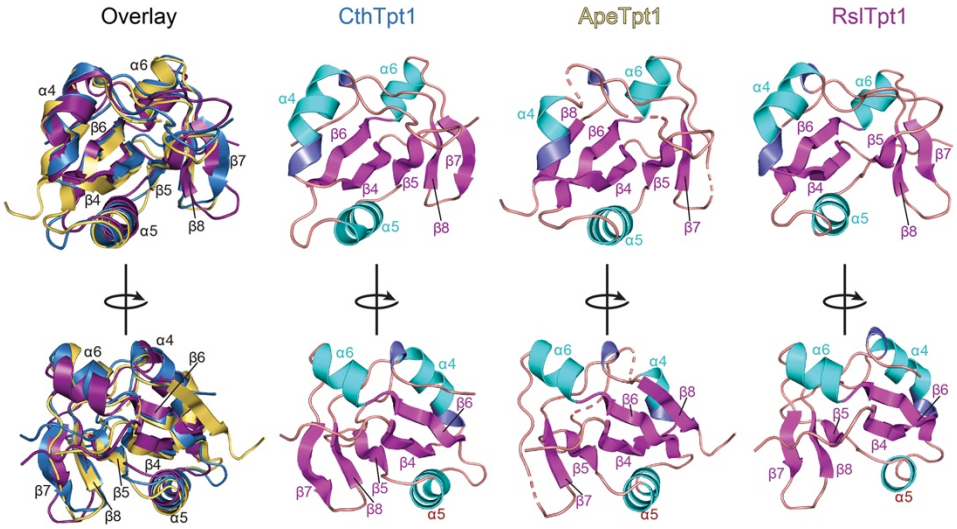

Figure S6. Comparison of the structures of the C-lobes of RslTpt1, CthTpt1 (1) and ApeTpt1 (2). The structural overlay includes residues 96-101, 103-112, 121-124, 128-138, 142-147, 148-154, 158-162, 165-168, 173-175 for RslTpt1; residues 98-103, 105-114,124-127, 130-140, 145-150, 151-157, 161-165, 168-171 and 176-178 for CthTpt1 (PDB: 6E3A, 6EDE); residues 93-98, 100-106, 108-109, 119-122, 125-135, 140-145, 146-152, 156-158, 160, 163-166, 171-173 for ApeTpt1 (PDB: 1WFX). The overlay includes a total of 224 backbone N, Cα, C' and O atoms. The extreme left panel shows the overlaid structures with CthTpt1 in blue, ApeTpt1 in yellow and RslTpt1 in magenta. Also shown are the individual structures in approximately the same orientation with key secondary structural elements labeled.

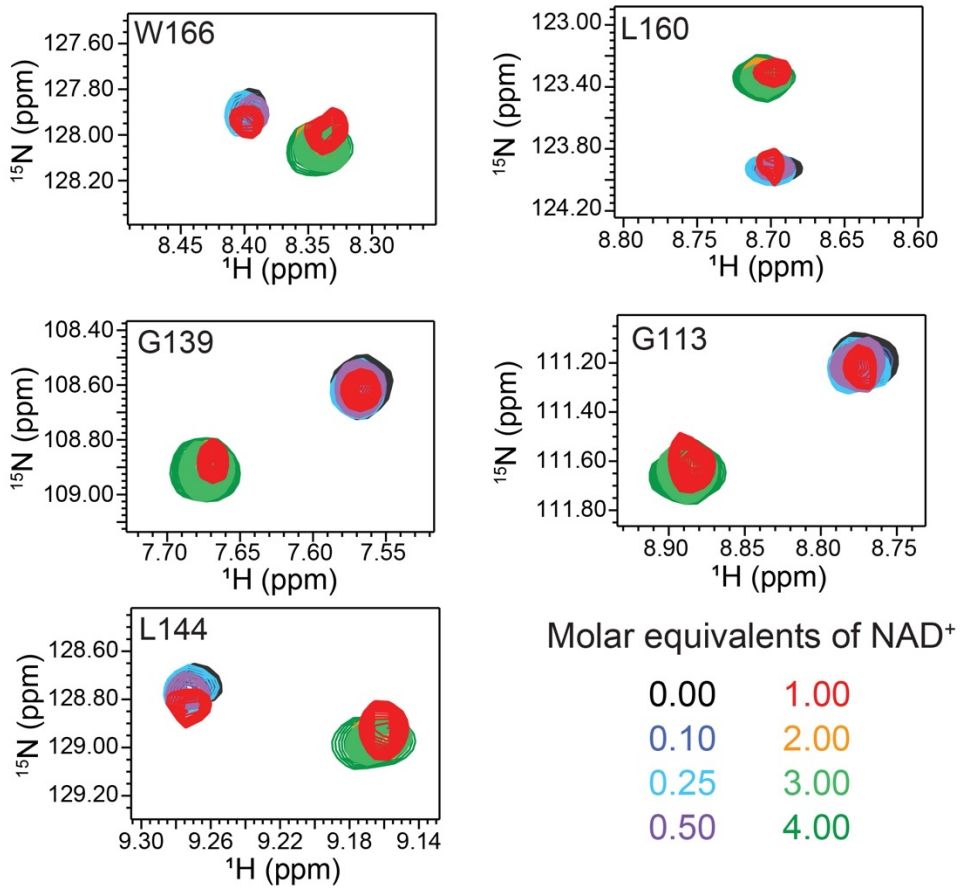

Figure S7. Representative well-resolved peaks from ^{1}H, ^{15}N HSQC spectra (900 MHz) of RslTpt1 in the presence of increasing amounts of NAD^{+}. Addition of NAD^{+} results in the reduction in intensity of peaks corresponding to apo-RslTpt1 and appearance of new peaks corresponding to the NAD^{+}-bound form indicating slow exchange on the chemical shift timescale.

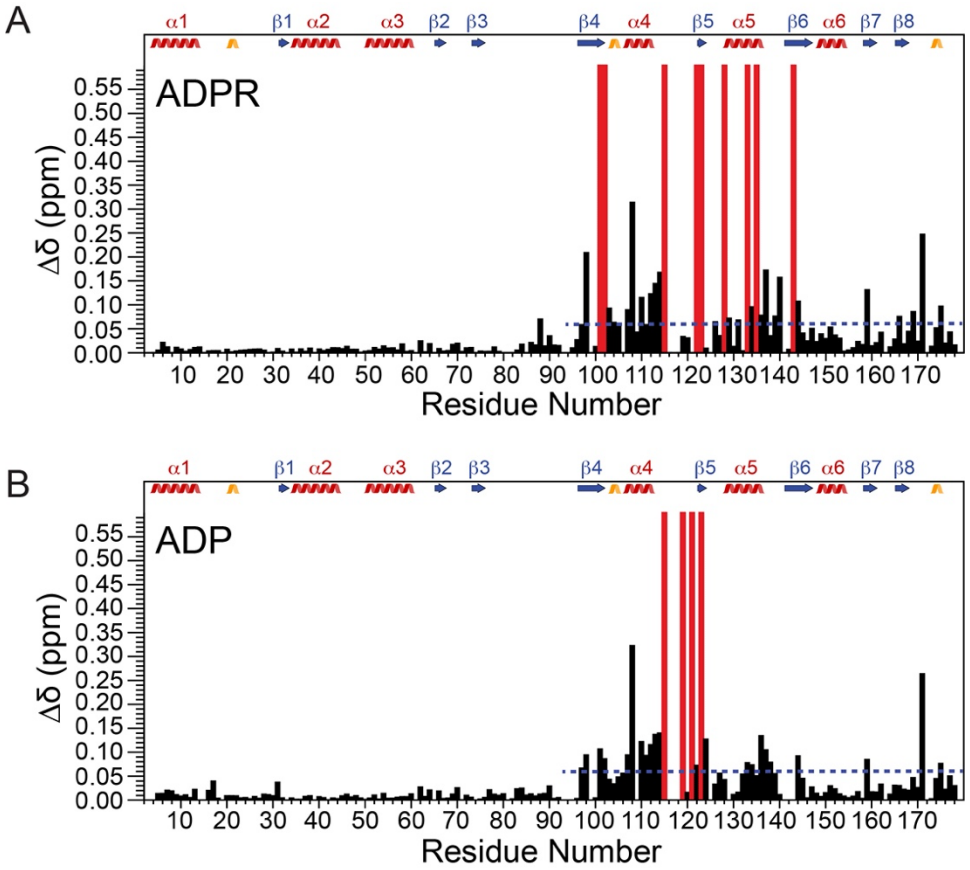

Figure S8. Chemical shift perturbations induced on the amide ^{1}H, ^{15}N resonances of RslTpt1 by 12 molar equivalents of ADPR (panel A) or ADP (panel B) are plotted along the amino acid sequence. Red bars indicate residues for which the corresponding resonances are perturbed but the chemical shifts for their final ligand-bound states could not be analyzed due to vanishing resonances, missing assignments, or spectral crowding. The blue dashed lines represent the average Δδ values for the C-lobe amide resonances in the presence of ADPR (0.06 ppm; the corresponding standard deviation = 0.06 ppm) and ADP (0.06 ppm; the corresponding standard deviation = 0.06 ppm). Resonances corresponding to the residues of the N-lobe are minimally perturbed in both cases. Secondary structural elements (definitions are as per apo-RslTpt1, see Table S3) are indicated; α-helices, β-strands and 3_{10}-helices are colored red, blue and gold, respectively. α-helices and β-strands are labeled.

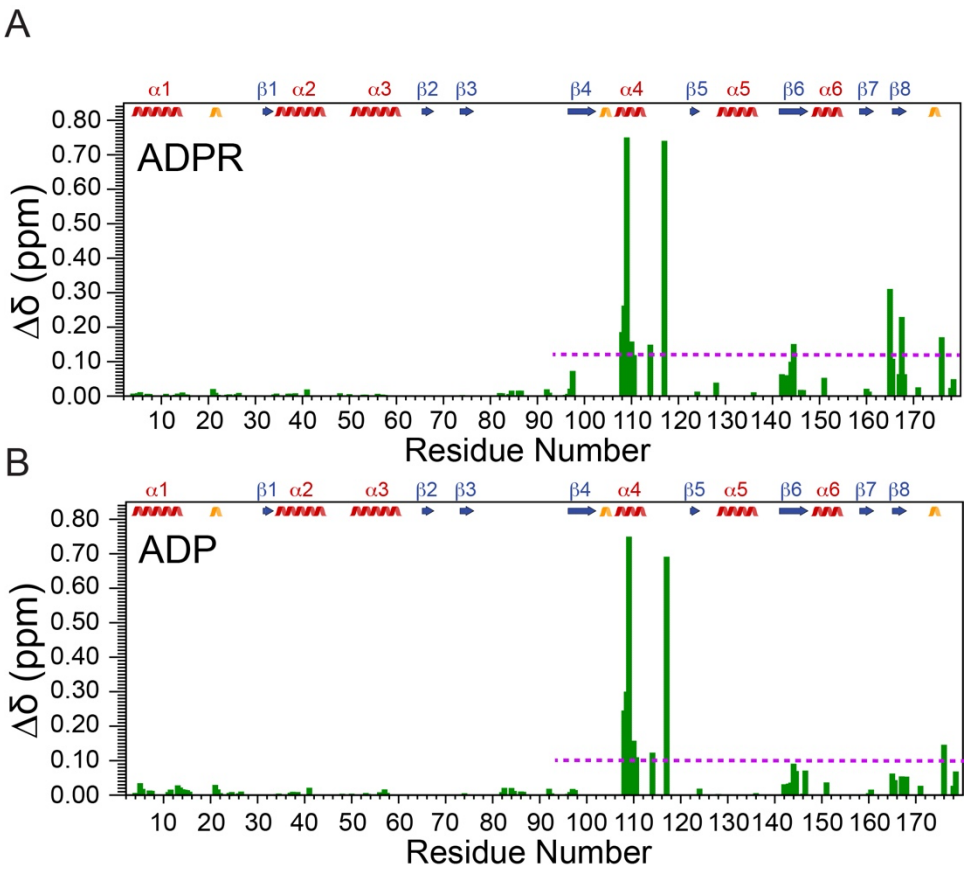

Figure S9. Chemical shift perturbations induced on the methyl ^{1}H, ^{13}C resonances of Ile (δ1), Leu, Val, and Met residues of RslTpt1 by 8 molar equivalents of ADPR (panel A) or ADP (panel B). The magenta dashed lines represent the average Δδ values for the C-lobe methyl resonances in the presence of ADPR (0.12 ppm; the corresponding standard deviation = 0.18 ppm) and ADP (0.10 ppm; the corresponding standard deviation = 0.17 ppm). As in the case of the backbone amides (see Figure S8), the ILVM methyl groups of the N-lobe residues are minimally perturbed. Secondary structural elements (definitions are as per apo-RslTpt1, see Table S3) are indicated; α-helices, β-strands and 3_{10}-helices are colored red, blue and gold, respectively. α-helices and β-strands are labeled.

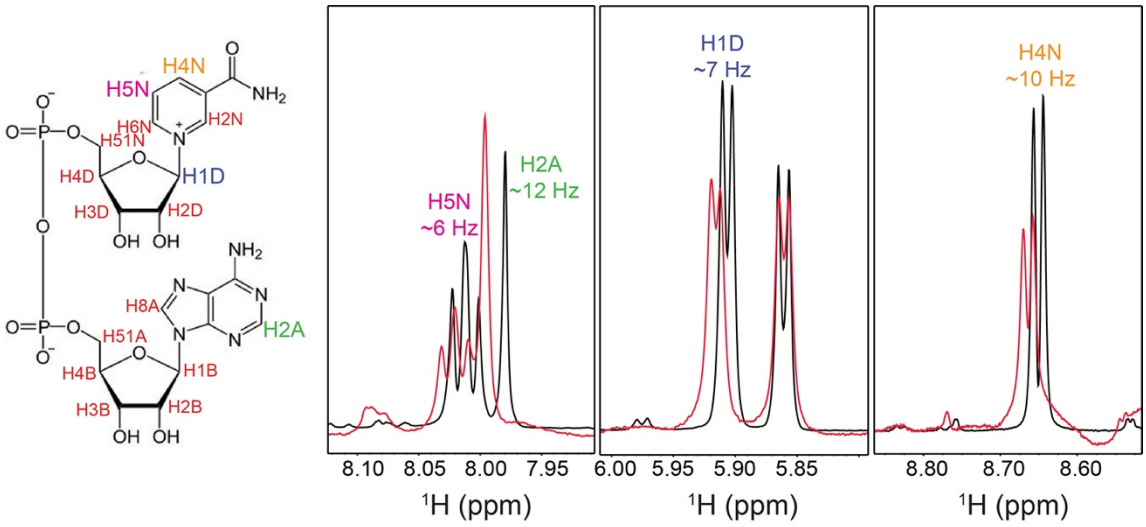

Figure S10. Representative traces illustrating chemical shift perturbations induced on NAD^+ resonances by the presence of 2 molar equivalents of unlabeled RslTpt1. The ^1H resonances of free NAD^+ and those in the presence of RslTpt1 are shown as black and red traces, respectively. The induced chemical shift perturbations (in Hz) are also indicated. The ^1H nuclei for which the perturbations are indicated in larger font on the chemical structure of NAD^+ on the leftmost panel. The atoms have been named as per IUPAC guidelines for structures determined by NMR spectroscopy (3).

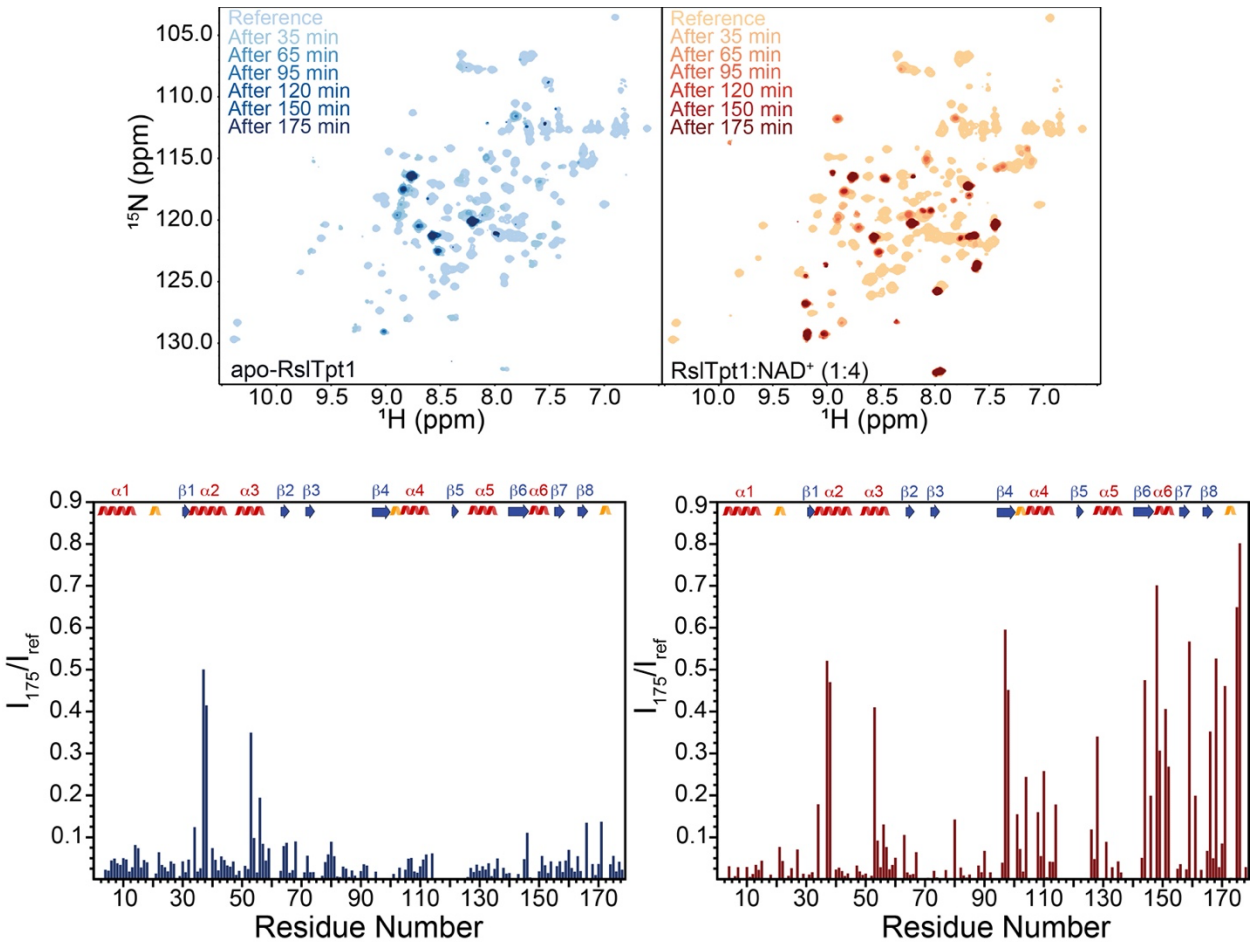

Figure S11. ^{15}N, ^{1}H HSQC spectra (700 MHz) of RslTpt1 acquired at various time intervals (alone, top left panel, and in the presence of 4 molar equivalents of NAD^+, top right panel) after dissolution in 100% D_2O-based NMR buffer. The bottom panels show plots of ratios of intensities (I_{175}) of corresponding resonances in the spectrum acquired 175 minutes after dissolution to that (I_{ref}) in the reference spectrum (acquired in H_2O-based NMR buffer containing 5% D_2O).

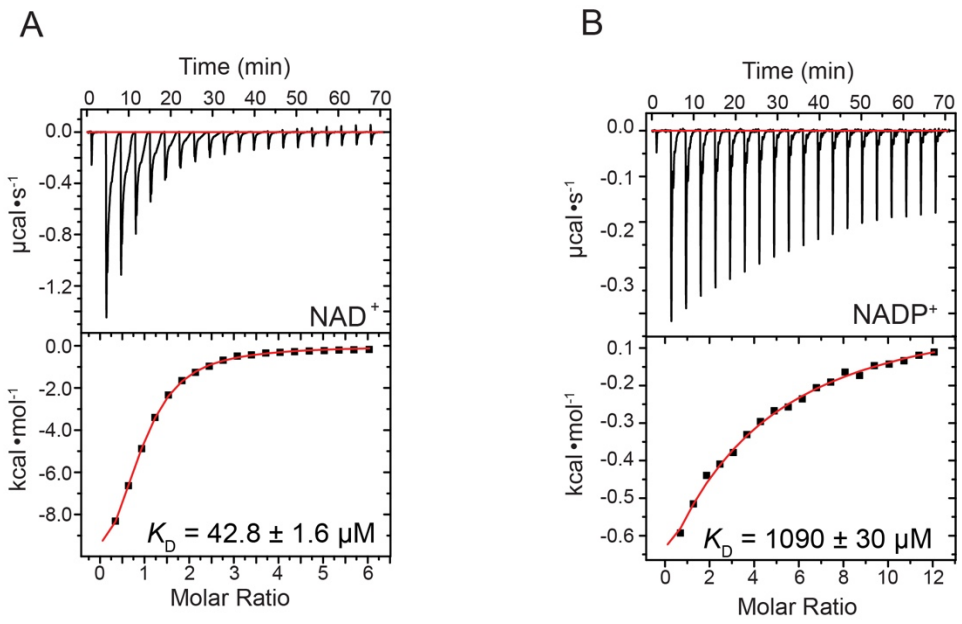

Figure S12. Representative ITC thermograms for the interaction of NAD^+ with RslTpt1 in the presence of saturating amounts of $NADP^+$ (panel A) and for the interaction of $NADP^+$ with RslTpt1 in the presence of the saturating amounts of NAD^+ (panel B). The affinities of each ligand towards RslTpt1 (NAD^+: $K_D = 47 \pm 3$ µM compared with 31 ± 1 µM; $NADP^+$: $K_D = 951 \pm 33$ µM compared with 1021 ± 53 µM; see Table 2) are not significantly altered in the presence of saturating amounts of the other. The K_D values, and corresponding standard deviations, indicated on the curves correspond to the fitted values for the specific trace shown.

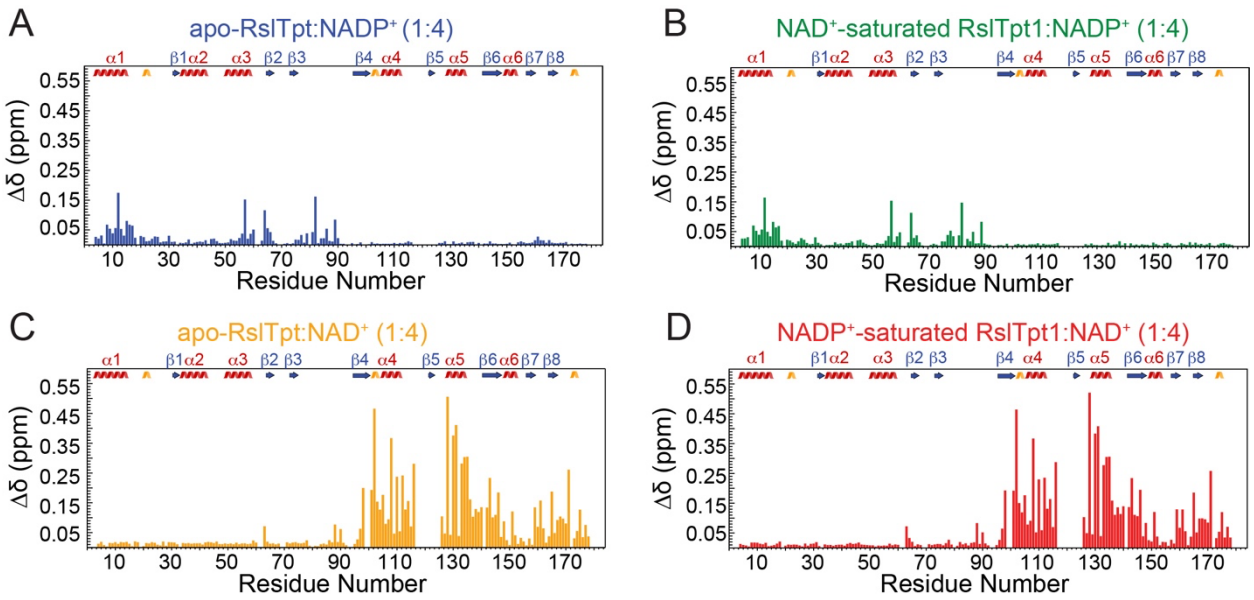

Figure S13. The chemical shift perturbations induced on the amide resonances of the N-lobe of RslTpt1 by $NADP^+$ (panel A) are unaffected by the presence of a saturating amount of NAD^+ (panel B). Similarly, the perturbations induced on the C-lobe of RslTpt1 by NAD^+ (panel C) are unaffected by the presence of a saturating amount of $NADP^+$ (panel D). Note that only those cases where numerical values for the perturbations could be obtained are shown; resonances that could not be compared due to line broadening, missing assignments or spectral crowding are not indicated. Secondary structural elements are indicated.

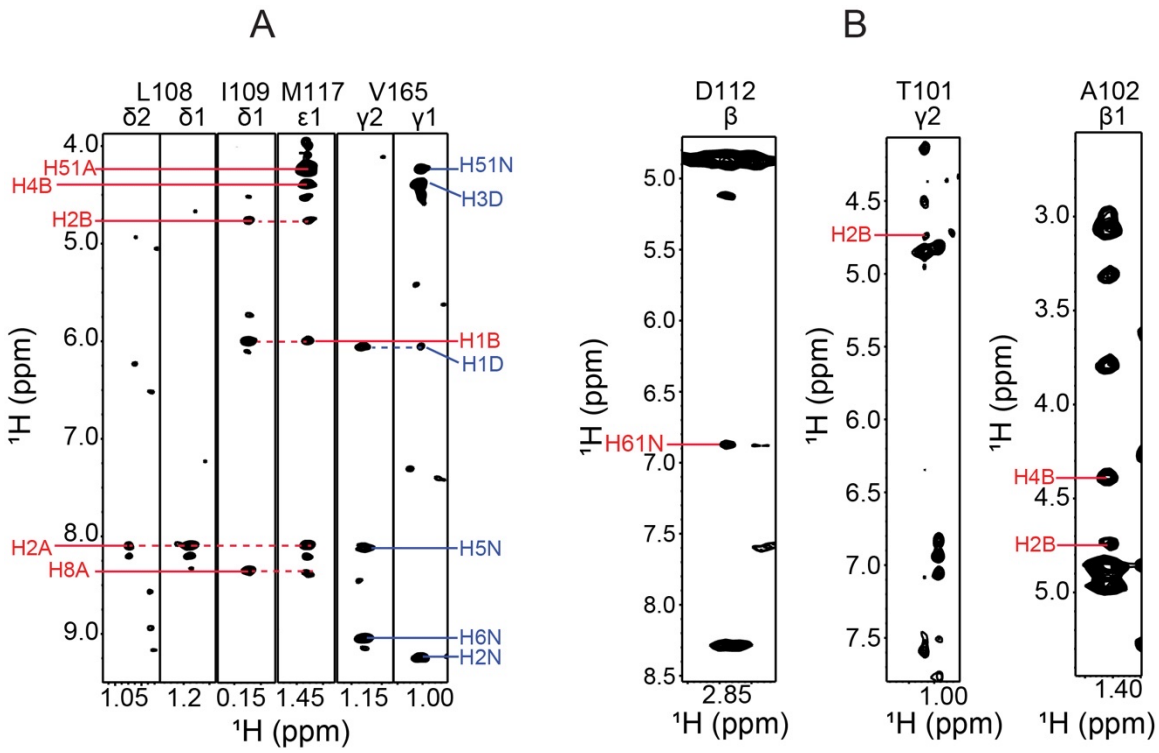

Figure S14. Representative strips through ^{13}C-methyl-edited (panel A) and ^{13}C-edited ^{1}H-^{1}H (panel B) NOESY spectra of RslTpt1 as part of the RslTpt1•NAD^{+} complex illustrating cross-peaks corresponding to inter-molecular contacts. Cross-peaks corresponding to the ADP-ribose moiety are labeled in red and those corresponding to the NMN moiety are labeled in blue.

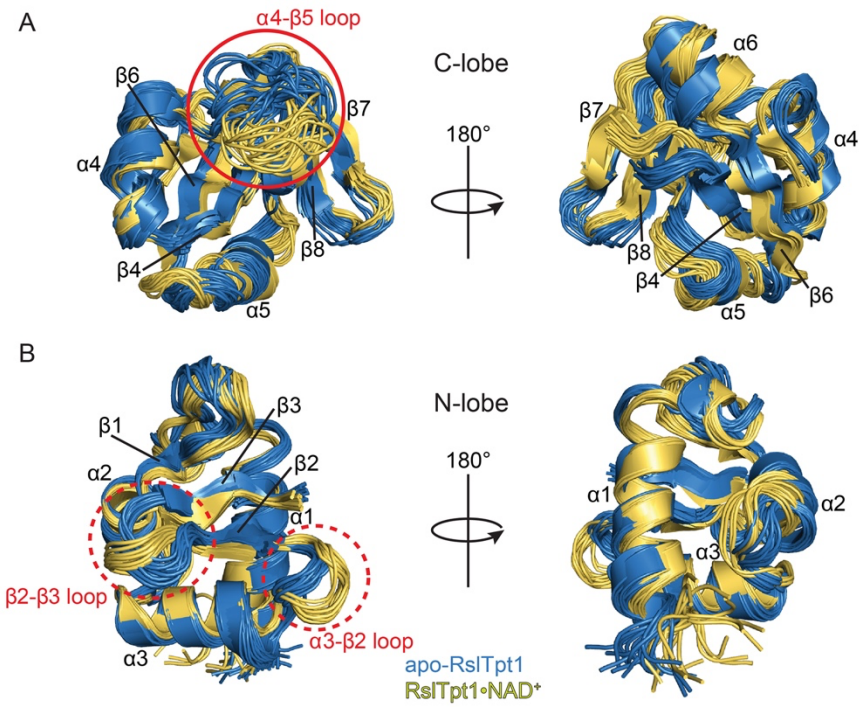

Figure S15. Comparison of the structures of the RslTpt1 C-lobe (panel A) and N-lobe (panel B) in the apo (blue) and the NAD^+-bound (yellow) states. Loop regions that show significant changes are indicated. For the C-lobe, the α4-β5 loop (indicated by the solid circle) shows a greater degree of closure in the bound state resulting from specific contacts with NAD^+. This region also shows large perturbations in resonance positions upon comparing the free and bound states. In contrast, the changes in the α3-β2 and β2-β3 loops of the N-lobe (indicated by the dashed circles in panel B) appear to reflect a limited number of structures chosen to represent the NMR ensemble. Inclusion of a 100 (instead of 20) structures to represent the NMR ensemble largely removes these differences suggesting that they reflect the force field and resultant energies rather than real differences within the NMR solution ensemble. The lack of substantial spectral perturbations in the presence of NAD^+ for the α3-β2 and β2-β3 loops lends further credence to this hypothesis.

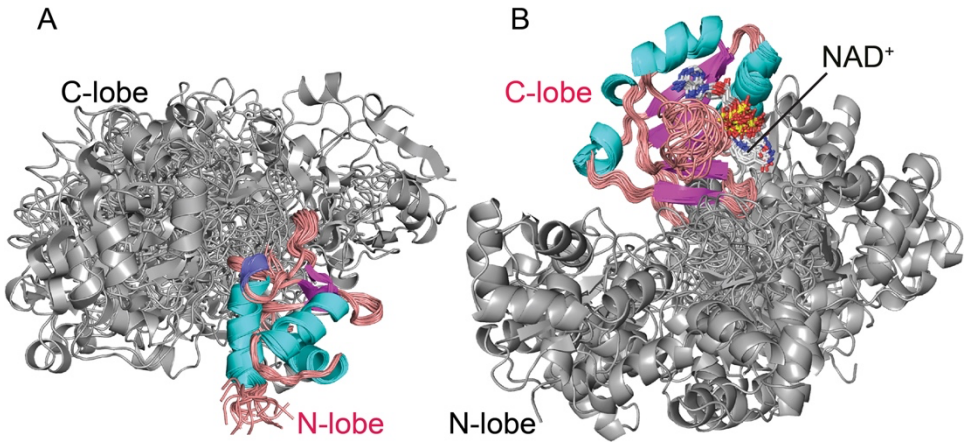

Figure S16. Structures of the NMR ensemble of the RslTpt1•NAD^+ complex overlaid with respect to their N-lobes (panel A) or their NAD^+-bound C-lobes (panel B). The aligned lobe is labeled in red font. As in the case of apo-RslTpt1, the inability to align the structures on both lobes simultaneously illustrates the fact that while the structures of the individual lobes are well-defined in solution, their relative orientation is not, indicative of significant inter-lobe flexibility.

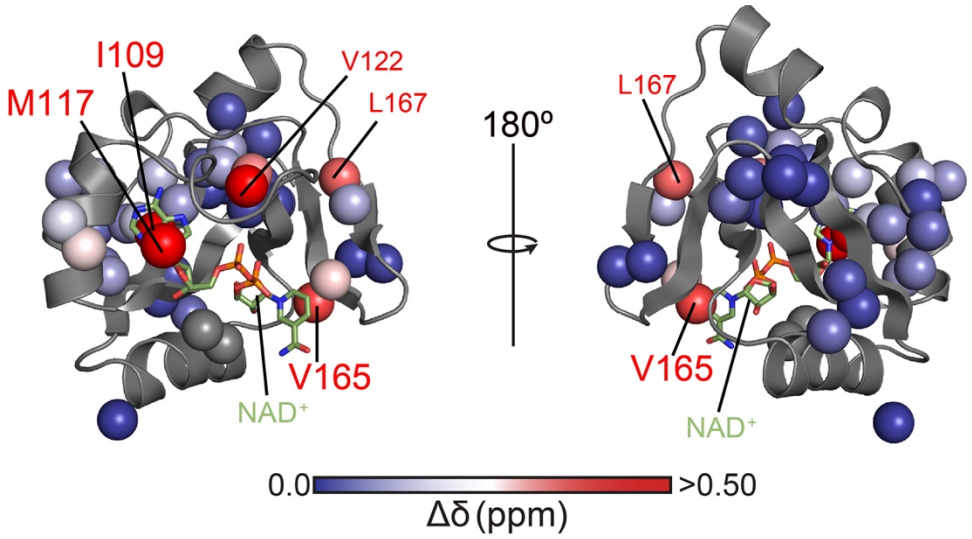

Figure S17. Chemical shift perturbations (CSPs) induced on the methyl resonances of Ile (δ1), Leu, Val, and Met residues on the C-lobe of RslTpt1 in the presence of NAD^+. The methyl groups are represented as spheres and colored based on the magnitude of the CSP using a blue to red gradient. Resonances that are observable in apo-RslTpt1 but are broadened out in the complex are assumed to display Δδ values > 0.50 ppm in this representation. Ile109 (0.8 ppm), Met117 (0.74 ppm), and Val165 (γ1/γ2: 0.43/0.29 ppm) that show the largest CSPs make close contact with NAD^+ in the RslTpt1•NAD^+ binary complex structure (these residues are labeled using larger font; see Figure 5B).

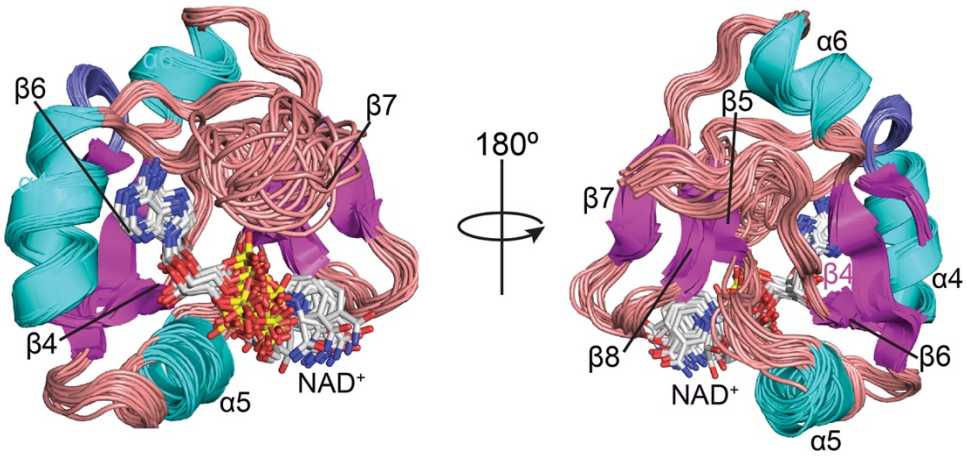

Figure S18. The NMR ensemble of the RslTpt1•NAD^+ complex showing NAD^+ with varying degrees of disorder when engaged to the C-lobe. The terminal nicotinamide moiety appears to show higher disorder within the ensemble compared to the adenosine moiety.

Table S1: Parameters used for the NMR experiments on apo-RslTpt1

	Direct			Indirect 1			Indirect 2			Field	NUS
Experiment	**Points**	**SW**	**Nucleus**	**Points**	**SW**	**Nucleus**	**Points**	**SW**	**Nucleus**		
HNCO	512	16	^{1}H	55	34	^{15}N	70	12	^{13}C	800	N
HN(CA)CO	512	12	^{1}H	55	34	^{15}N	70	12	^{13}C	800	Y
HNCA	1024	16	^{1}H	26	34	^{15}N	44	26	^{13}C	800	N
CBCA(CO)NH	512	12	^{1}H	55	34	^{15}N	80	64	^{13}C	800	Y
HNCACB	512	12	^{1}H	55	34	^{15}N	80	64	^{13}C	800	Y
CC(CO)NH	512	12	^{1}H	55	34	^{15}N	64	70	^{13}C	800	Y
HC(CCO)NH	512	12	^{1}H	55	34	^{15}N	80	7.8	^{1}H	800	Y
CCH-TOCSY	512	12	^{1}H	64	70	^{13}C	64	70	^{13}C	800	Y
HCCH-TOCSY	512	12	^{1}H	64	70	^{13}C	128	8.2	^{1}H	800	Y
^{15}N-HSQC-NOESY	1024	16	^{1}H	31	34	^{15}N	55	10	^{1}H	800	N
^{13}C-HSQC-NOESY (D_2O)	512	12	^{1}H	64	70	^{13}C	128	12	^{1}H	900	N
^{13}C-HSQC-NOESY-aromatic (D_2O)	512	12	^{1}H	24	30	^{13}C	135	11	^{1}H	800	N
^{13}C-HSQC-NOESY-aromatic	512	12.5	^{1}H	27	30	^{13}C	124	12.5	^{1}H	700	N
^{13}C methyl HMQC-NOESY-HMQC	512	12.5	^{1}H	70	19	^{13}C	120	19	^{13}C	600	N

Points indicate the number of complex points; sweep-widths (SW) are in ppm; field indicates the ^{1}H frequency in MHz. Use of non-uniform sampling is indicated by a “Y” in the NUS column.

Table S2: Parameters used for the NMR experiments on the RslTpt1•NAD^+ complex

	Direct			Indirect 1			Indirect 2			Field	NUS
Experiment	**Points**	**SW**	**Nucleus**	**Points**	**SW**	**Nucleus**	**Points**	**SW**	**Nucleus**		
HNCO	512	13	^{1}H	74	32	^{15}N	144	10.5	^{13}C	600	N
HN(CA)CO	512	13	^{1}H	84	32	^{15}N	144	10.5	^{13}C	600	Y
HNCA	512	12	^{1}H	32	34	^{15}N	64	32	^{13}C	800	Y
HN(CO)CA	512	12	^{1}H	45	34	^{15}N	70	32	^{13}C	700	Y
CBCA(CO)NH	512	12	^{1}H	32	34	^{15}N	64	70	^{13}C	800	Y
CBCANH	512	12	^{1}H	45	34	^{15}N	70	70	^{13}C	700	Y
HBHA(CO)NH	512	12	^{1}H	45	34	^{15}N	64	6	^{1}H	800	Y
CC(CO)NH	512	12	^{1}H	45	32	^{15}N	100	68	^{13}C	600	Y
HC(CCO)NH	512	13	^{1}H	45	32	^{15}N	128	7.2	^{1}H	600	Y
CCH-TOCSY	512	12	^{1}H	64	67	^{13}C	64	67	^{13}C	800	Y
HCCH-TOCSY	512	12	^{1}H	60	67	^{13}C	120	8.2	^{1}H	800	Y
^{15}N-HSQC-NOESY	512	12	^{1}H	31	34	^{15}N	128	12	^{1}H	800	N
^{13}C-HSQC-NOESY	512	11.4	^{1}H	36	67	^{13}C	100	11.4	^{1}H	700	N
^{13}C-HSQC-NOESY (D_2O)	512	12	^{1}H	40	67	^{13}C	135	11.8	^{1}H	800	N
^{13}C-HSQC-NOESY-aromatic	512	13	^{1}H	32	30	^{13}C	128	13	^{1}H	800	N
^{13}C-HSQC-NOESY-aromatic (D_2O)	512	13	^{1}H	32	30	^{13}C	128	13	^{1}H	800	N
^{13}C methyl HMQC-NOESY-HMQC	512	12.5	^{1}H	70	19	^{13}C	70	19	^{13}C	800	N
^{13}C methyl NOESY-HMQC	384	6	^{1}H	29	19	^{13}C	45	6	^{1}H	700	N

Points indicate the number of complex points; sweep-widths (SW) are in ppm; field indicates the ^{1}H frequency in MHz. Use of non-uniform sampling is indicated by a "Y" in the NUS column.

Table S3:
Consensus secondary structure elements for apo-RslTpt1 and the RslTpt1•NAD$^+$ complex[a]

	apo-RslTpt1	RslTpt1•NAD$^+$ complex
α-helix		
α1	5-14[b]	5-15[b]
α2	34-44	34-44
α3	50-60	50-59
α4	106-112	103-112[c]
α5	128-136	128-135
α6	148-154	148-153
3_{10}-helix		
1	20-22	19-21
2	103-105	-[c]
3	173-175	173-175
β-strand		
β1	32-33	32-33
β2	65-67	66-67
β3	73-76	73-75
β4	96-102	100-102
β5	122-124	122-124
β6	141-147	141-146[d]
β7	158-161	158-161
β8	165-168	165-168
β9	-	176-177[e]

[a]Consensus secondary structure elements were calculated using STRIDE (4) and present is at least 80% of the structures in each NMR ensemble.
[b]The first 4 residues in the RslTpt1 construct represent a remnant of the purification tag after cleavage.
[c]The Glu103-Asn105 segment that forms a 3_{10} helix in apo-RslTpt1 incorporates into a longer α4 in the RslTpt1•NAD$^+$ complex (residues Glu103-Asp112).
[d]β6 is distorted at Leu144 in many of the constituent structures of the RslTpt1•NAD$^+$ complex.
[e]β9 is formed in only ~40% of the structures comprising the apo-RslTpt1 ensemble; β9 is formed in all structures in the ensemble representing the RslTpt1•NAD$^+$ complex.

REFERENCES

1. Banerjee, A., Munir, A., Abdullahu, L., Damha, M.J., Goldgur, Y. and Shuman, S. (2019) Structure of tRNA splicing enzyme Tpt1 illuminates the mechanism of RNA 2'-PO4 recognition and ADP-ribosylation. *Nature Commun.*, **10**, 218.
2. Kato-Murayama, M., Bessho, Y., Shirouzu, M. and Yokoyama, S. (2005) Crystal structure of the RNA 2'-phosphotransferase from *Aeropyrum pernix* K1. *J. Mol. Biol.*, **348**, 295-305.
3. Markley, J.L., Bax, A., Arata, Y., Hilbers, C.W., Kaptein, R., Sykes, B.D., Wright, P.E. and Wuthrich, K. (1998) Recommendations for the presentation of NMR structures of proteins and nucleic acids. IUPAC-IUBMB-IUPAB Inter-union task group on the standardization of data bases of protein and nucleic acid structures determined by NMR spectroscopy. *J. Biomol. NMR*, **12**, 1-23.
4. Frishman, D. and Argos, P. (1995) Knowledge-based protein secondary structure assignment. *Proteins*, **23**, 566-579.